6624 *Macromolecules* **2009**, *42*, 6624–6632
DOI: 10.1021/ma901010d

Macromolecules
ARTICLE

Viscoelasticity and Shear Stability of Single-Walled Carbon Nanotube/Unsaturated Polyester Resin Dispersions

Matthew J. Kayatin and Virginia A. Davis*

Department of Chemical Engineering, Auburn University, Auburn, Alabama 36849

Received May 8, 2009; Revised Manuscript Received July 7, 2009

ABSTRACT: We report a detailed investigation of the effects of concentration and surface chemistry on the dispersion and rheological properties of single-walled carbon nanotubes in isophthalic unsaturated polyester, a prevalent thermoset resin. The growth of the SWNT network was shown by the concentration-dependent crossover parameters which provided an empirical basis for mastercurve scaling. To the author's knowledge, this is the first report of this type of colloidal scaling for dispersed SWNTs. Rheological percolation was found to occur at 0.106 vol % ± 2% by using both power-law scaling and the concentration-dependent yield stress. The average effective hydrodynamic aspect ratio for the dispersed SWNTs was ~650. The SWNTs were found to be dispersed as small non-Brownian aggregates whose low shear aggregation behavior was strongly dependent on intermolecular interactions related to SWNT surface oxygen content.

Introduction

The extraordinary mechanical, electrical, and thermal properties of individual single-walled carbon nanotubes (SWNTs) and multiwalled carbon nanotubes (MWNTs) have been well documented in the literature.[1] The complement of excellent physical properties coupled with low mass density and high length to diameter ratio (aspect ratio) make carbon nanotubes (CNTs) desirable alternatives to traditional micrometer-scale fillers (e.g., glass fibers) in polymer composites.[2] Furthermore, CNT dispersions exhibit low electrical and rheological percolation thresholds, allowing electrical and mechanical property enhancement at low loadings.[3] CNTs are geometrically unique in that their surface area per unit volume provides an enormous means of communication with any continuous phase, giving rise to great opportunity for effective load transfer.[4] In spite of this fact, mechanical property improvements have typically been lower than predicted or reported inconsistently with respect to theoretical expectations.[5−7] The potential for mechanical property enhancement is determined by both the degree of nanomaterial dispersion throughout the composite system and interfacial adhesion between the polymer matrix and dispersed phase.[8,9] Poorer than expected properties are a consequence of not only a less than ideal dispersion state but also the dominance of interfacial interactions. As the defining length scales of the filler and polymer converge, these interactions must be given careful consideration.[10] A truly "ideal dispersion" state is classified by complete exfoliation of the individual CNTs from bundles or clusters. However, in the literature the term "ideal dispersion" is sometimes used to describe a dispersion in which individual tubes coexist with small aggregates[11] as SWNTs readily form undesirable aggregates as a result of their highly polarizable and pristine sp^2-hybridized carbon interface.[12,13] The pairwise interaction of parallel CNTs exhibits a deep potential energy well at equilibrium separation on the order of 20−40 k_BT/nm,[13−15] making them inherently difficult to process as individuals. Thermodynamically, this attractive potential results in a large, positive free energy of mixing favoring only dilute solutions of pristine tubes in most solvents.[16] It has been shown that the enthalpy of mixing is the limiting factor controlling solubility and can be expected to be positive for most pristine nanotube−polymer mixtures.[17] Thus, significant research has focused on improving dispersion through mixing and sonication as well as increasing nanotube−solvent compatibility using covalent or noncovalent functionalization techniques.[18−20]

The rheological and mechanical properties of CNT-based composites depend on CNT dispersion state, aspect ratio and orientation of nanotubes, and interactions between nanotubes and polymer molecules.[21] Therefore, understanding the rheological response of CNTs in fluids is of the utmost importance for rational design of polymer processing parameters. The rheological response of CNTs has been studied in a variety of polymer solutions, melts, and solvents; in spite of the broad differences in solvent nature, some remarkable parallel behaviors have been observed. Several investigations have revealed SWNT rigid-rod behavior under steady and oscillatory shear in superacids,[22,23] surfactants,[24] and melts.[25] Furthermore, direct individual particle tracking measurements of fluorescently tagged SWNTs in aqueous sodium dodecyl sulfate have shown that they behave as Brownian rods with a persistence length on the order of 20 μm,[26] consistent with theoretical expectations.[27] Less ideal polymeric solvents have also been studied to reveal concentration-dependent yielding behavior manifested via an elastic network[28] and Bingham fluid behavior in concentrated aqueous dispersions.[29] The effect of prolonged shear mixing time on the emergence of dispersion elasticity has also been established.[30]

With respect to thermoset nanocomposite systems, a number of studies have utilized high shear mixing strategies to disperse CNTs in various resins, most commonly in epoxies.[5,31−34] Fan and Advani revealed the variation in rheological behavior upon loading, aspect ratio, and initial dispersion quality supporting the utility of oscillatory shear for probing dispersion state.[11] Similarly, Rahatekar et al. made direct connections between rheological response and fluid microstucture using a shear-optical technique.[32] In addition, Ma et al.'s modeling of aggregated suspensions in epoxy confirmed a rheological dependence on both orientation and dispersion state under rotational shear,

*Corresponding author: Tel 334-844-2060; fax 334-844-2063; e-mail davisva@auburn.edu.

 Published on Web 07/22/2009

providing great insight toward dispersion dynamics.[35] However, in spite of the fact that unsaturated polyester resin (UPR) has historically represented a 2 times larger U.S. market share than epoxy resins over the past three decades,[36] there have only been limited investigations of CNT dispersions in UPR.[37−39] Presumably, the paucity of efforts to disperse SWNTs in UPR and perform rheological characterization is a result of the reported difficulties associated with loss of the styrene monomer contained in most UPRs and undesired polymerization.[40] In any case, a detailed study of CNT dispersions while preserving initial UPR composition has been absent from the literature.

We report the shear dispersion of SWNTs into UPR matrix and the effect of nanotube concentration on sample viscolelasticity. Specifically, we focus on the evolution of a developing network structure by tracking the network crossover modulus which we use to demonstrate universal scaling of the system through a colloidal scaling technique. We also compare the results of multiple methods for determining the onset of rheological percolation. Finally, we investigate the effect of subtle changes in SWNT surface chemistry on low shear aggregation. These results provide new fundamental insights into SWNT−UPR dispersions that can help guide SWNT−UPR nanocomposite development and processing.

Experimental Section

Materials. Polylite X31003-00 base resin (Lot #4508-38) comprising of 40 wt % styrene monomer and 60 wt % proprietary isophthalic polyester was used as received from Reichhold, Inc. (Durham, NC). The resin was Newtonian with a neat viscosity of 2 Pa s at 20 °C. Multiple reactor batches of SWNTs produced by the high-pressure carbon monoxide (HiPco) process at Rice University (Houston, TX) and Unidym, Inc. (Menlo Park, CA) were used in this work. HiPco batch 183.6 was received partially purified (65 wt % SWNT) following a deactivated thermal oxidation process,[41] and this raw material is referred to as sample u183.6. The purification method was completed at Auburn via Soxhlet extraction in $HCl_{(aq)}$ to a SWNT purity of 98−99 wt %; this purified sample is referred to as SWNT p183.6. Rice purified HiPco batch 187.3 (92−93 wt % SWNT) and Unidym Lot #P0355 (91−92 wt % SWNT) were used as received. For all samples, the final impurities were primarily residual iron catalyst.

Characterization Methods. SWNT purity was measured with a TA Instruments (New Castle, DE) Q500 thermal gravimetric analyzer (TGA). All samples were vacuum-dried overnight. The sample chamber was purged with 60 cm^3/min of compressed air. The temperature was held at 120 °C to further remove residual water, ramped at 10 °C/min to 800 °C, and held at this temperature for 45 min.

Raman spectra were obtained using a Renishaw (Hoffman Estates, IL) inVia Raman microscope affixed with a Leica 50× (0.75 NA) objective. Samples were irradiated using 514 and 785 nm lasers. A total of 10 scans from a Raman shift of 3200−100 cm^{-1} were collected with a 10 s sample exposure time under ambient conditions.

X-ray photoelectron spectroscopy (XPS) was performed to study SWNT surface chemistry in a custom Kratos Analytical XSAM 800 surface analysis system using unmonochromatized Mg Kα (1253.6 eV) X-ray radiation and a hemispherical energy analyzer. SWNT samples were dried for ∼18 h under vacuum at ∼105 °C and cooled under vacuum before analysis. An exhaustive list of calibration and XPS analyzer details for the exact instrument used in this research can be found elsewhere.[42,43] Because of specimen charging, the energy axis of each XPS spectra was shifted to make the C 1s binding energy line equal to the standard hydrocarbon energy of 284.6 eV. The uncertainty of the recorded binding energies was ±0.1 eV. Overall binding energy scans from 0 to 600 eV were performed. Surface compositions were calculated using peak backgrounds determined by the iterative Shirley technique, and instrument specific corrections were applied. High-resolution XPS peak positions for specific carbon bound functionalities in SWNTs were obtained from the literature.[44−48]

Optical microscopy was performed using a Nikon (Melville, NY) Eclipse 80*i* optical microscope using a Nikon 60× (1.40 NA) oil immersion objective and a 10× (0.3 NA) objective. A 2× magnification was also applied before the camera doubling the effective magnification. A Zeiss EM 10C 10CR transmission electron microscope (TEM) was also used to study SWNT−UPR sample dispersions. Samples were diluted in acetone directly in the shear mixer and stirred gently so as to wash the sample but not further separate the SWNTs. This solution was then dropped onto a 300 mesh carbon-coated copper grid from Electron Microscopy Sciences (Hatfield, PA).

Dispersion. CNT dispersions were formulated by mass fraction based on measured component weights. Volume fractions were calculated using a UPR density of 1.09 g/mL (manufacturer specified) and assuming a HiPco SWNT mass density of 1.45 g/mL. Shear mixer components were purchased from Ace Glass (Vineland, NJ). Appropriate amounts of material were added to a 50 mL round-bottom flask, and the jointed head was sealed with Teflon after an argon purge. A Teflon stirring blade (1.85 cm radius) was affixed offset to a 10 mm Teflon-coated, steel stirring shaft. The stirring shaft was driven using a $^1/_4$ hp solid state laboratory stirrer, and the mixer was run at ∼1000 rpm for a minimum of 72 h. The maximum shear stress, estimated at the flask wall, was on the order of 3 kPa when operated at angular velocity of $\sim 10^2$ rad/s. The estimated shear stress is conservatively low since large shear gradients and turbulent flow are likely present in areas where the stirring blade approaches the flask wall due to its offset configuration. The flask was immersed in a room temperature water bath. Aliquots above 0.010 vol % loading were extracted using a bulb and pipet having a wide inner diameter of 7 mm to limit shear alignment of the CNTs. Dilute samples of 0.010 vol % and below were drawn using a 7.5 in. long, 12 gauge syringe (Sigma-Aldrich), sealed in a vial, and allowed to relax for 24 h. Sample concentrations ranged from 0.003 to 0.250 vol % (0.004 to 0.332 wt %).

Rheometry. Rheological measurements were performed using a Anton Paar (GmbH) Physica MCR 301 rheometer having a torque transducer sensitivity of 0.1 μN m. Sample temperature and atmosphere were controlled using a Peltier temperature control device and Peltier upper oven[49] counter-cooled at 20 °C. Primarily, a 50 mm diameter cone and plate measuring geometry with cone angle of 2.018° was used. Only where indicated, a 43 mm diameter quartz parallel plate was used. The cone truncation and distance between the center of the upper and lower surfaces was constant at 52 μm for all measurements; at this gap the required sample volume was 1.14 mL. Measurements were taken at 20 °C in order to limit styrene evaporation. For oscillatory measurements, a sinusoidal varying strain wave $\gamma = \gamma_0 \sin(\omega t)$ of amplitude γ_0 was imposed on the sample, and the steady-state stress response was measured as a function of angular frequency, ω. The stress wave was of the form $\tau = \gamma_0[G' \sin(\omega t) + G'' \cos(\omega t)]$, where G' and G'' represent the storage and loss modulus, respectively. The damping factor $\tan(\delta)$ was $\tan(\delta) = G''(G')^{-1}$. Additionally, the magnitude of the complex modulus, G^*, was defined as $|G^*| = (G'^2 + G''^2)^{1/2}$ and the complex viscosity, η^*, as $|\eta^*| = |G^*|\omega^{-1}$. All oscillatory measurements were performed within the linear viscoelastic regime which was experimentally determined using controlled frequency, variable strain measurements. For steady shear measurements, the flow was viscometric with constant shear rate $\dot{\gamma}$. The Reynolds number, $Re = \dot{\gamma} z^2 \rho \eta_s^{-1}$, was always less than unity, where η_s represents the neat solvent viscosity and z the mean sample gap.

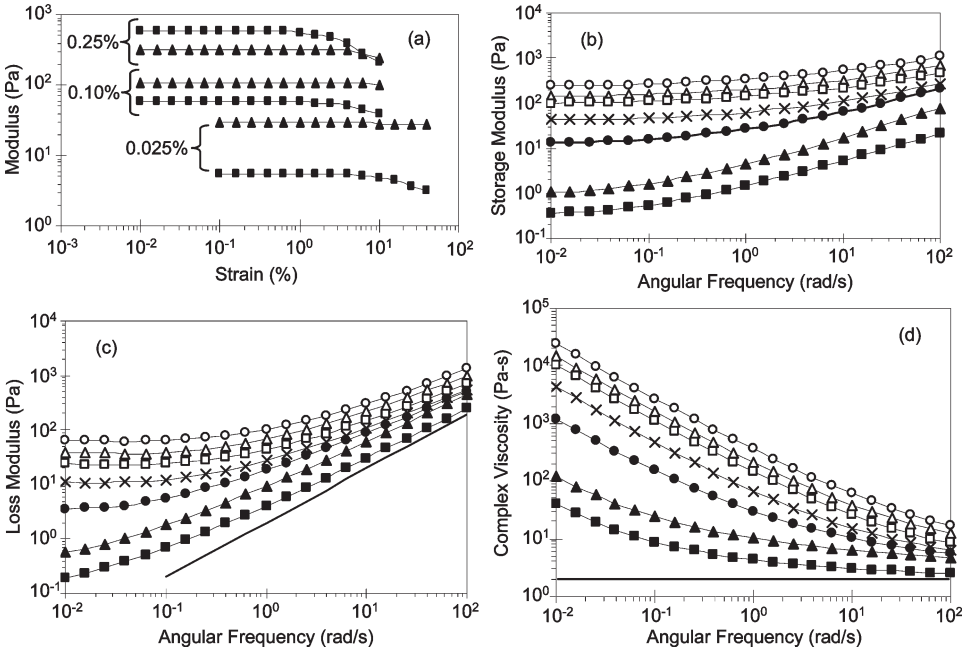

Figure 1. (a) Characterization of linear viscoelastic regime for three concentrations showing storage [squares] and loss [triangles] moduli with variable strain. (b) Storage modulus G' with varying angular frequency, (c) corresponding loss modulus G'', (d) complex viscosity η^* determined from viscoelastic moduli. Thin solid lines in (c) and (d) represent neat UPR. Symbols are (■) 0.025, (▲) 0.050, (●) 0.100, (×) 0.147, (□) 0.183, (△) 0.200, and (○) 0.250 vol %.

Results and Discussion

Viscoelastic Behavior. Figure 1 displays the viscoelastic behavior of SWNT p183.6 dispersions at concentrations ranging from 0.025 to 0.250 vol %. Typical response curves used for characterization of the linear viscoelastic (LVE) strain limit are shown in Figure 1a with $\omega = 10\,s^{-1}$ shown for three SWNT loadings. With increasing SWNT concentration the critical strain limit of the linear viscoelastic regime decreased from ~5% strain at 0.025 vol % to ~0.5% at 0.250 vol %, indicating an increase in the complexity of the fluid structure.[24] The difference between G' and G'' decreases with increasing concentration; for both 0.025 and 0.100 vol % SWNT the response was dominated by G'' showing character of the UPR, while for the 0.250 vol % the behavior was dominated by the elastic response of the SWNT network. This behavior can be conveniently described by examining the LVE damping factor which has a value of ~5.29 for 0.025 vol % and decreases to ~1.88 at 0.100 vol %, indicating a decrease in viscous response. At 0.250 vol %, where G' emerges as the dominant modulus, the damping factor is ~0.53, indicating the fluid's increased elasticity at this concentration and frequency of observation.

A plot of the frequency-dependent storage modulus is shown in Figure 1b; the magnitude of G' increases with loading, accompanied by a flattening in the slope of the response. This frequency-independent behavior at low ω is indicative of increasing solidlike elastic response. In addition, the distinct jump in the low-frequency magnitude of G' between 0.050 and 0.100 vol % is indicative of percolation. This jump is also reflected in the low-frequency loss modulus (Figure 1c). Even at high concentrations the slope of G'' is still existent at frequencies above ~0.5 rad/s, showing some viscous response from the UPR solvent. The complex viscosity is displayed by Figure 1d; the transition in behavior is evidenced by both an enhanced resistance to flow and increased degree of shear thinning. Remarkably, a 4 orders of magnitude enhancement in zero-shear viscosity was observed at a SWNT loading of only 0.183 vol %.

In order to provide insight into the developing structure of the fluid, the concentration and time dependence were removed from the viscoelastic moduli using the colloidal scaling technique established by Trappe and Weitz for weakly attractive carbon black dispersions.[50] To the author's knowledge this is the first report of this behavior for SWNT dispersions, and its successful application indicates that the SWNTs behaved as attractive colloidal particles. The viscoelastic crossover points, where G' and G'' are of equal magnitude, provided the basis for the scaling. This crossover behavior is believed to be a result of the relaxation mode associated with the developing SWNT network in the fluid[25] and is defined by a common viscoelastic modulus, G_c, for a unique crossover frequency, ω_c. Figure 2a shows the trend in crossover parameters for each concentration, increasing in magnitude and shifting to a higher frequency with increased SWNT loading. Remarkably, the behavior of this intrinsic parameter was found to be quite reproducible as evidenced by the error bars showing the range of experimental values. As displayed by Figure 2b, scaling the concentration-dependent LVE moduli by their concentration-dependent crossover parameters G_c and ω_c results in two master curves for G' and G'', intersecting at unity. To the right of unity the response is viscous, dominated by G'', showing character of the UPR. Conversely, to the left of unity the response is dominated by G' and converges to a single modulus as a result of the SWNT structure present in the fluid. For reference, the loss modulus for neat UPR is shown by the thin black line; by comparison to G''/G_c the SWNT dispersion data show restricted solvent mobility. At high reduced frequencies, there exists a slight discrepancy in the data trend; G'' is higher and G' is lower in magnitude for the 0.025 vol % loading (squares) with respect to the 0.050 vol % loading (triangles). While this slight discrepancy is within the range of experimental error, it may be the result of an underdeveloped SWNT network structure in the fluid below the percolation threshold. Excluding this data set, the high-frequency behavior was fit to a power law; the data

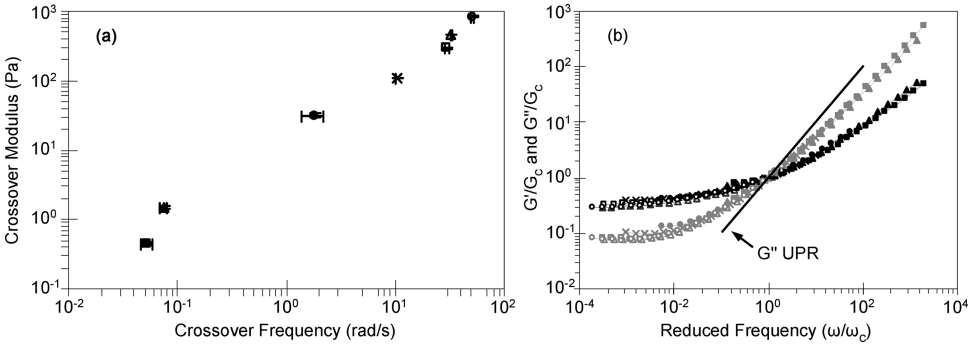

Figure 2. (a) Concentration-dependent crossover modulus and crossover frequency used to scale the (b) reduced storage [black] and loss [gray] moduli with varying angular frequency. The thin black line in (b) represents G'' for neat UPR. Error bars indicate experimental range of values. Symbols for concentration are consistent with Figure 1.

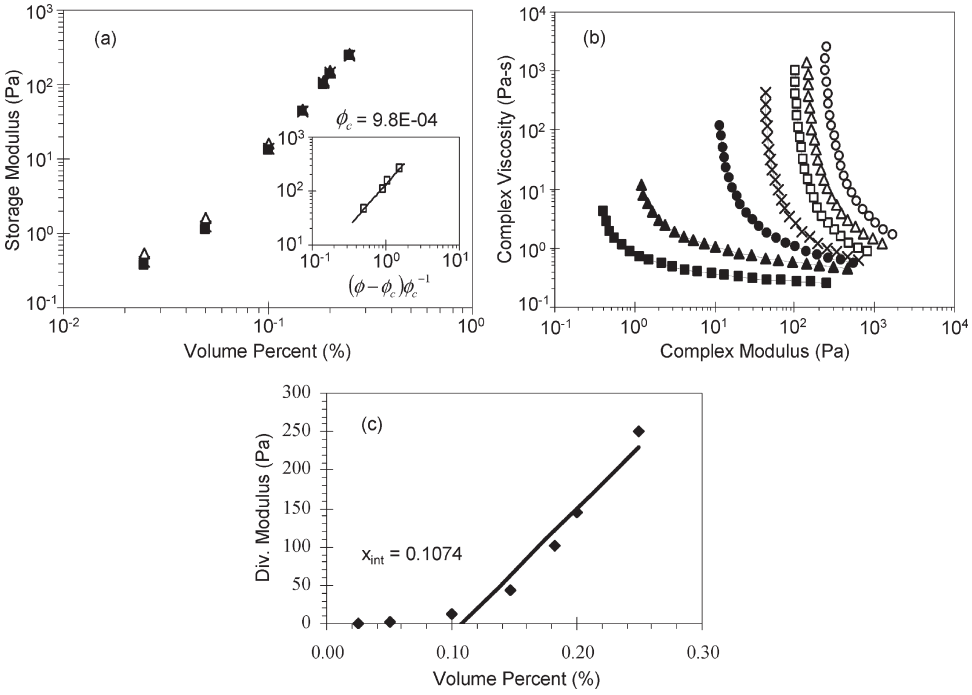

Figure 3. (a) Storage modulus with varying SWNT loading plotted at angular frequencies of (■) 0.01, (×) 0.0398, and (△) 0.10 rad/s with the inset (a) showing power law scaling for 0.10 rad/s data. (b) Divergence plot showing development of yield stress. Symbols for concentration are consistent with Figure 1. (c) Divergent modulus against loading with a linear fit for yield behavior.

scale as $G''/G_c \propto (\omega/\omega_c)^{0.85}$ and $G'/G_c \propto (\omega/\omega_c)^{0.63}$ over high angular frequencies. This reduced scaling is markedly similar to, but slightly weaker than, the exponents of 0.9 (G'') and 0.7 (G') found by Hobbie and Fry for shear aggregated dispersions of fractal MWNTs;[28] they used a different criterion for selecting their scaling parameters and obtained the relaxation time by forcing a horizontal axis shift. Conversely, in the present study we extracted this data from the crossover frequency which required no assumption a priori. However, due to differences in the concentration regimes between the two studies, the behavior of the scaling parameter alone with respect to CNT loading cannot readily be compared.

Rheological Percolation. A quantitative understanding of the critical concentration ϕ_c required for nanotube percolation is necessary since the optimum balance between nanotube loading and mechanical reinforcement exists near this transition. Significantly below ϕ_c there is insufficient fluid structure to provide considerable mechanical and/or electrical property enhancement. However, significantly above ϕ_c intertube spacing can be so decreased as to promote nanotube aggregation and thus result in mechanical property degradation by means of local stress defects.[51] The previously described jumps in G' and η^* between 0.050 and 0.100 vol % provide a first approximation for ϕ_c. In order to obtain a more exact value, two other methods for determining ϕ_c were compared: power law scaling and development of an apparent yield stress.

Near the percolation threshold, the following power law holds

$$G' \propto (\phi - \phi_c)^n \quad (1)$$

where ϕ is the SWNT loading and n is the scaling exponent. Figure 3a displays the trend in low-frequency G', plotted at three constant angular frequencies, as a function of SWNT loading. In order to shift the horizontal axis to be centered around unity, a slight variation of the classic power law

shown by Du et al. was used.[21] The data in Figure 3a were fit by adjusting ϕ_c in accordance with

$$G' \propto \frac{(\phi - \phi_c)^n}{\phi_c} \quad (2)$$

The inset of Figure 3a shows data taken at $\omega = 0.10$ rad/s graphically fit to the power law by maximizing the regression coefficient R^2, resulting in $\phi_c = 0.098$ vol % with a critical exponent of $n = 1.55$. Similarly, for $\omega = 0.01$ rad/s, $\phi_c = 0.095$ vol % with $n = 1.6$. Martin et al. suggested the possibility that error in estimating the CNT density may skew the power law parameters when using volume fraction as the adjustable parameter.[52] Therefore, the power law scaling shown by the inset of Figure 3a was also performed using weight fraction as the adjustable parameter, resulting in the critical mass fraction for percolation $x_c = 0.0014$ at $\omega = 0.01$ rad/s. This value of x_c translates to a $\phi_c = 0.105$ vol %, which is a difference of only ~10%; thus, any error associated with SWNT density appears to be reasonable in this case. The observed scaling exponent of $n = 1.55$ is weaker than value of ~2.1 expected for chemical gels, where bonds resist stretching but are free to rotate under strain.[53] Hu et al. found $n = 1.5$ for MWNTs in a thermoplastic melt; however, no explanation was given toward the origin of its magnitude.[54] Additionally, a slope of 1.6 has been previously observed for SWNTs in 102% H_2SO_4 but was attributed to the SWNTs only being weakly attractive due to the reduction in van der Waals potential resulting from SWNT protonation.[55] In the present case, the exponent may be influenced by the presence of SWNT-rich and UPR-rich phases as described by Kota et al.'s interpenetrating phase percolation model.[56] The low shear aggregation tendency of some low-concentration SWNT dispersions described in the subsequent section would also be consistent with the presence of a SWNT-rich phase. Finally, we note that it is possible the value of 1.55 may be related to an experimental artifact linked to CNT orientation introduced by the required sample extraction from the shear mixer and transfer to the rheometer; due to the volatility of the styrene component in the UPR, allowing many hours of relaxation after loading was not practical. Other researchers have noted the effect of sample prestressing[24] as well as the long equilibrium relaxation times required postloading.[25]

Determination of the percolation threshold based on the development of an apparent yield stress was recently shown by Mitchell and Krishnamoorti, who extracted the effective aspect ratio of dispersed nanotubes from a divergence plot.[57] A plot of the overall flow resistance η^* against the overall deformation resistance G^* is shown in Figure 3b and reveals a divergent complex modulus behavior. An order of magnitude decrease in η^* at a constant value of G^* is interpreted as yield behavior and appears at $\phi \geq 0.100$ vol %. The observance of an apparent yield stress with no zero-shear viscosity plateau (Figure 1c) is attributed to the long relaxation time of the CNT network with respect to the time scale of experimental observation. This yielding behavior becomes more pronounced and shifts to higher yield stresses with increasing concentration; at $\phi = 0.250$ vol % the fluid withstands a stress of ~250 Pa, and nearly a 3 orders of magnitude drop in η^* is observed. The divergent complex modulus shown by Figure 3b is plotted against SWNT loading in Figure 3c, and the x-intercept is taken to be the critical concentration resulting with $\phi_c = 0.107$ vol %. Remarkably, this value is within 2% from ϕ_c obtained by the power law method; the average of these values provides a reasonable estimate of ϕ_c to be 0.106 vol %. On the basis of this value of ϕ_c and geometric percolation model theory,[58] the effective aspect ratio of the SWNTs in UPR is $L/d = 555$.[57] Using the isotropic concentrated phase transition $\phi_i \sim \pi d(4L)^{-1}$ given by the theory of Doi and Edwards results in $L/d \sim 740$.[59] The 30% difference between these two values originates from the fact that Doi and Edwards consider excluded volume interactions whereas the geometric percolation model does not; neither approach accounts for aspect ratio polydispersity. The estimated aspect ratios are reasonable for individually dispersed SWNTs, but both TEM images and the dilute rheological behavior suggest that this aspect ratio represents non-Brownian SWNT bundles.

Dilute Behavior. In contrast to higher concentration dispersions of SWNT p183.6, over the range from 0.003 to 0.010 vol % viscous response was observed under oscillatory shear with no crossover parameter or low frequency elasticity (see Supporting Information). Measurements characterizing the start-up of flow were carried out with a SWNT loading of 0.005 vol % in an effort to determine the time required for steady-state viscosity. Figure 4a shows an overlay of the transient viscosity data under constant shear. Interestingly, at low shear rates, over long time scales, no steady-state viscosity was achieved. Instead, near the time one would expect to achieve steady state (~10^3 s) under a shear rate of 10^{-3} s^{-1} the viscosity shows an asymptotic behavior. Increasing shear rate in a stepwise fashion to 10^{-2} s^{-1} and then 10^{-1} s^{-1} reveals a breakdown of this response followed by almost no deviation from neat UPR viscosity at 10^0 s^{-1}. This behavior suggests there exists a critical shear stress for dispersion of aggregates formed under weak shear similar to that observed by Chaouche and Koch for non-Brownian fiber suspensions,[60] and this critical stress may be necessary to overcome the effects of both mechanical entanglement and particle attractive forces.[28] The fact that the data in Figure 4a were collected at very dilute concentrations suggests the strong influence of long-range attractions between the dispersed SWNTs. Such interactions can be expected on the basis of the large van der Waals attraction between SWNTs and the relatively long-range scaling of van der Waals attractions between cylinders.[61] Long-range attractions between SWNTs have also been experimentally observed in a number of other systems.[62]

The origin of the transient viscosity behavior was confirmed to be low shear aggregation by performing start-up of flow experiments between quartz parallel plates. Divergent low shear start-up behavior has been observed previously for semidilute non-Brownian nanotube dispersions by Lin-Gibson et al. and studied rheo-optically.[63] Remarkably, the aggregation behavior of p183.6 was strong enough to be observed by the naked eye (see Supporting Information) at sample gaps greater than ~0.344 mm. At smaller gaps, the asymptotic low shear viscosity response remained, but the structures could only be observed with aid of magnification; a shear aggregated dispersion of p183.6 (0.005 vol %) carefully extracted from these plates was observed using transmitted light optical microscopy (Figure 4b), revealing a striated structure of UPR-rich areas. The gap height dependence on domain size is consistent with previous observations for non-Brownian MWNT suspensions.[63] As a result of shear-induced aggregation, we were unable to measure the steady-state viscosity of the sample. Characterization of the complex viscosity of the samples was feasible, and removing the concentration

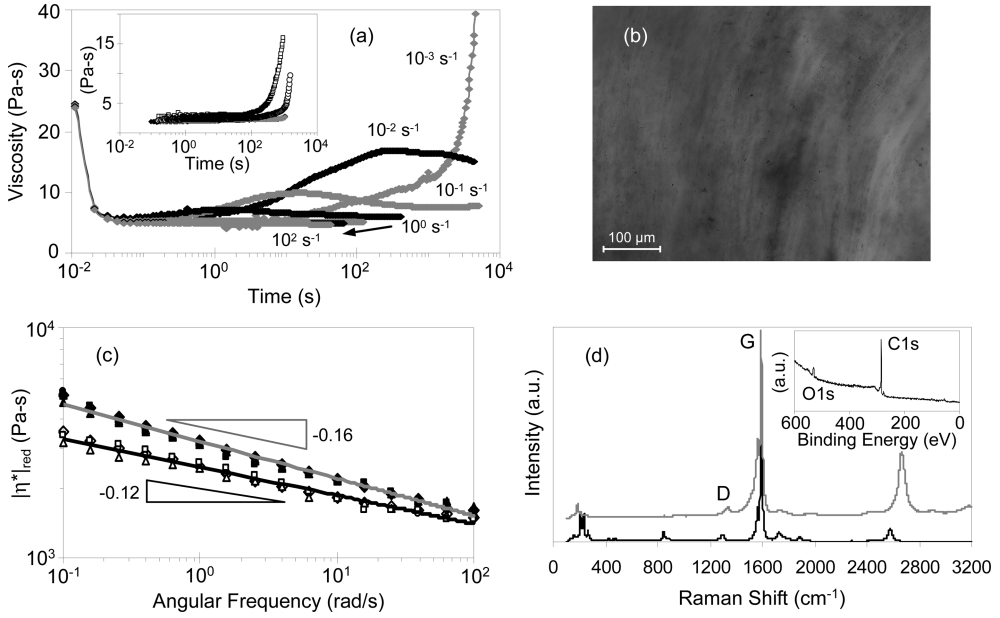

Figure 4. (a) Start-up of flow for batch p183.6 under constant shear rates ramped from low to high. Inset of (a) showing aggregation behavior for samples 183.6 (□) and P0355 (○) at 0.01 s^{-1}. (b) Optical micrograph of shear aggregated p183.6 SWNTs (0.005 vol %) under 10× (0.3 NA) magnification with 2× magnification in front of the camera. (c) Reduced complex viscosity for dilute dispersions of p183.6 [closed symbols] and 187.3 [open symbols]. Concentrations are (◆) 0.010, (●) 0.007, (▲) 0.005, and (■) 0.003 vol %. (d) Typical Raman spectra for batch u183.6 under 514 nm (top, gray) and 785 nm (bottom, black) irradiation. The inset of (d) shows a typical overall XPS scan for u183.6.

dependence on this response yields the reduced complex viscosity

$$|\eta^*_{red}| = \frac{|\eta^*| - \eta_s}{\phi \eta_s} \quad (3)$$

where ϕ is the sample volume fraction. Figure 4c shows the reduced data for SWNT p183.6, which showed low shear aggregation, and 187.3, which did not aggregate under steady shear. The slope of the reduced data is significantly lower than that expected for Brownian rods, and no viscosity plateau is observed. This result suggests the SWNT dispersions are behaving as non-Brownian entities; exploration of shear frequencies both above and below the typical experimental range failed to exhibit any change in slope. Estimation of the rotational Peclet number[64]

$$Pe = \frac{\dot{\gamma} \pi \eta_s L^3}{3 k_B T (\ln(L/d) - 0.8)} \quad (4)$$

under $\dot{\gamma}$ of 10^{-1} s^{-1} (Figure 4c), where L^3 is the nanotube swept volume calculated from length L and k_BT is the thermal energy, results in Pe on the order of 10^1, indicating the imposed shear stress is dominant over the rotational diffusivity under experimental conditions. We make use of the average hydrodynamic aspect ratio of ~650 calculated previously and purposely underestimate the contour length to be on the order of 1 μm. On the basis of this analysis, the collective evidence of non-Brownian behavior is compelling; non-Brownian behavior supports the ease of repeatability of in measuring crossover parameters (Figure 2a), long sample relaxation times, and importance of shear history in these dispersions.

Origin of Aggregation Behavior. Simulation has shown that flow-induced aggregation can occur in non-Brownian fiber suspensions as a result of fiber friction alone.[65] In order to determine the exact origin of shear-induced aggregation in the SWNT-UPR samples, additional nanotube dispersions were created at 0.005 vol % from a variety of SWNTs including batch u183.6, P0355, and 187.3. A summary of the characteristics of each SWNT batch is found in Table 1. The inset of Figure 4a shows the start-up behavior at a constant shear rate of 10^{-2} s^{-1}. Intriguingly, only two samples show evidence of low shear aggregation behavior, p183.6 and P0355. Figure 4c shows that the slopes of the reduced complex viscosity versus frequency for the p183.6 (aggregating) and 187.3 (nonaggregating) samples are quite similar, indicating that differences in the flow behavior are unlikely to be the sole cause of sample aggregation. Comparative analysis of sample surface chemistry was performed by means of XPS scans, as shown by the inset of Figure 4d. For all samples the main surface constituents were only carbon and oxygen. The results of the overall energy scans reveal a trend in surface chemistry with shear aggregation behavior as summarized by Table 1. Interestingly, samples p183.6 and P0355, which showed shear-induced aggregation, had low surface oxygen atomic concentration of ~1%. On the other hand, samples stable under low shear, batches 187.3 and u183.6, showed significant surface oxygen contents of 5% and 8%, respectively. In order to gain insight into the origin of the surface bound oxygen, high-resolution XPS scans of the C 1s orbital were compared, along with comparisons from Raman spectra and sample purity. High-resolution C 1s scans of the SWNT samples exhibiting shear aggregation are displayed by Figure 5a and show little structure on the high-energy side of the curve (> 284.6 eV)

Table 1. Summary of Various SWNT Sample Properties[a]

sample	% CNT	Agr	% O	D/G_{514}	D/G_{785}
p183.6	98−99	y	1	~0.06	~0.04
u183.6	~65	n	8	~0.06	~0.04
187.3	92−93	n	5	~0.16	~0.12
P0355	91−91	y	1	~0.17	~0.07

[a] % CNT: SWNT sample purity; Agr: indication if sample shows shear aggregation; % O: percent atomic surface oxygen content; D/G_{514}: D-peak to G-peak Raman intensity under 514 nm irradiation; D/G_{785}: D-peak to G-peak Raman intensity under 785 nm irradiation.

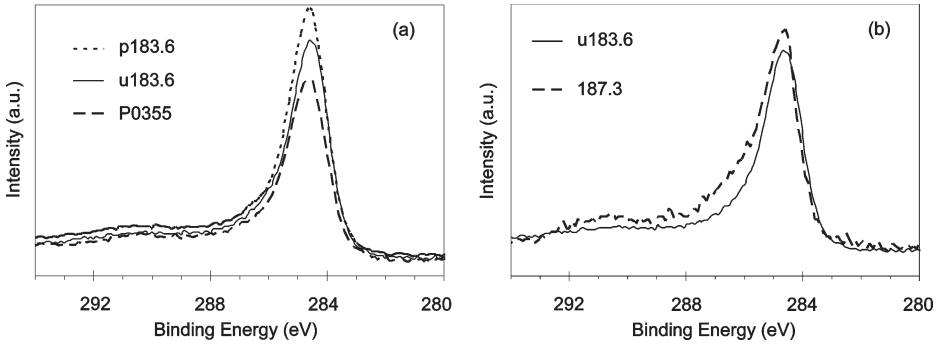

Figure 5. (a) Overlay of high-resolution XPS scans for samples showing similar photoelectron emission on high-energy side (> 284.6 eV) of the C 1s curve, indicating absence of surface bound oxygen to carbon. (b) Overlay of samples having significant atomic oxygen concentrations, as determined by overall binding energy scans.

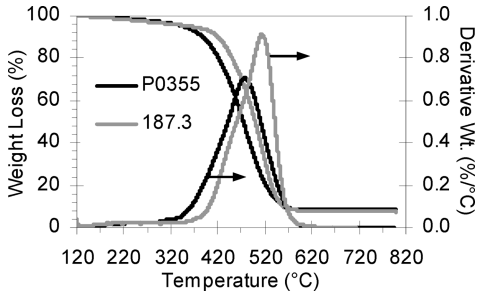

Figure 6. Overlay of TGA curves for batch 187.3 and P0355. The derivative weight loss with temperature is indicative increased amorphous carbon impurity in P0355.

where oxygen-containing functional groups would be found, consistent with their low surface oxygen content of ~1%. Interestingly, the C 1s scan for batch u183.6 also shows little structure, suggesting its surface oxygen content in not covalently bound to carbon. This hypothesis was confirmed by comparison of the D-peak to G-peak Raman intensity ratio $I(D)/I(G)$ of SWNT 183.6 before and after purification. The D-band (~1350 cm^{-1}) scattering results from symmetry breaking defects of a graphene sheet while the G peak (~1590 cm^{-1}) is associated with sp^2 carbon vibrations in the axial direction.[66] Figure 4d shows a typical Raman spectrum for sample u183.6. Intensity ratios before (0.05−0.07 for 514 nm and 0.03−0.04 for 785 nm) and after (0.06−0.07 for 514 nm and 0.03 −0.05 for 785 nm) purification show little to no change. Thus, the observed surface oxygen content of 8% is attributed to the presence of 35 wt % sample impurities consisting of both residual catalyst and disordered carbon based on TGA (see Supporting Information); the impurities also impart stability under low shear from steric retardation of van der Waals attractive forces. $I(D)/I(G)$ ratios for the P0355 SWNTs, which showed aggregation, were increased (0.15−0.20 for 514 nm and ~0.07 for 785 nm) with respect to batch p183.6 and comparable to values for batch 187.3 (0.15−0.17 for 514 nm and ~0.12 for 785 nm), which was stable under weak shear. The origin of these significant $I(D)/I(G)$ ratios are a result of sidewall and/or end defect sites or the presence of amorphous carbon in the sample.[67] In this case, the potential effect of sample impurities can be eliminated since both the P0355 SWNTs (91−92 wt %) and batch 187.3 (92−93 wt %) showed similar TGA degradation curves and had similar residual mass; the derivative weight loss as a function of temperature for both samples is shown in Figure 6. The overall weight percentage loss indicates that oxidation initiates at a lower temperature in batch P0355 SWNTs. In fact, the derivative weight loss curves peak at 480 °C for batch P0355 and 517 °C for batch 187.3. This 37 °C difference in peak weight loss was attributed to increased presence of disordered carbon in the P0355 sample. Previous measurements on the thermal oxidation of SWNTs indicate that amorphous carbon burns at ~365 °C,[68] and with increasing SWNT purity thermal stability increases and peak losses shift toward the true SWNT ignition temperature of ~600 °C.[69] Thus, defect sites/amorphous carbon present in the P0355 SWNT sample were not sufficient to prevent aggregation alone. In contrast, batch 187.3 was stable against shear aggregation even though it had less carbon impurities, indicating the importance of sample surface chemistry.

Evidence for the effect of surface chemistry on aggregation behavior is further enhanced by examining the C 1s curves in Figure 5b which show the high-resolution photoelectron emission for batch 187.3 against batch u183.6. The high-energy side of the curve for batch 187.3 shows "structure" at a binding energy of ~286.1 eV. The presence of increased emission at this energy is characteristic of phenolic or hydroxyl functionalities, indicating the observed surface oxygen content of 5% was from oxygen-containing groups bound to carbon. Additionally, carbonyl groups located at ~287.7 eV may be present. There was no indication of carboxylic acid functionalities (~289.1 eV) in any of the aforementioned samples. The presence of surface groups containing singularly bound oxygen atoms appears to impart increased dispersion stability; there is tremendous opportunity for intermolecular association through hydrogen bonding with oxygen atoms attached to the oligomer backbone. Thermodynamically, the benefit of these groups is twofold: they reduce the enthalpy of mixing both by decreasing the intertube van der Waals binding energy[17] and by increasing favorable solute−solvent interactions. This effect is intricate in that intermolecular association via hydrogen bonding also serves to reduce system entropy; these effects will be explored in future work. It is noted that attempts to disperse acid oxidized SWNTs in UPR failed. Physically, this phenomenon can be attributed to the presence of carboxylic acid functionalities existing as their conjugate base which is incompatible with the isophthalic polyester (structure shown in Supporting Information).

Conclusions

The intention of this work was to provide a detailed rheological study of the high shear dispersion of single-walled carbon nanotubes in a viscous unsaturated polyester resin. Specifically, we focused on the bulk fluid viscoelastic property enhancement resulting from the developing nanotube microstructure. To this end, the response of the viscoelastic moduli with varying nanotube concentration was studied, and the developing network's

crossover modulus proved to be very insightful in providing a basis for colloidal mastercurve scaling. The resulting mastercurves showed two separate subtypes of rheological response. At concentrations below the percolation threshold, the response suggested a developing nanotube network structure, whereas at higher concentrations a saturated and elastic network structure was observed. These observations were correlated with the onset of rheological percolation which was found to be comparable based on several methods, including a recently proposed technique of tracking the evolution of yield stress. To provide more insight into the dispersion flow behavior, dilute samples were characterized, revealing that they existed as non-Brownian aggregates that exhibited surface chemistry-dependent low-shear aggregation behavior. Surface analysis and comparative measurements indicated oxygen-rich functionalities were capable of providing dispersion stability, and our findings suggest hydroxyl and/or phenolic groups helped prevent nanotubes from reaggregation. Physically, the ability for these functional groups to hydrogen bond with the isophthalic polyester structure supports this conclusion. In summary, these results provide a foundation for further study of the dispersion of carbon nanotubes in an important class of polymers as well as provide insights into future directions for tailoring nanotube surface chemistry in this system.

Acknowledgment. We thank the The Richard E. Smalley Institute for Nanoscale Science and Technology at Rice University for providing SWNTs and Reichold for providing the polyester resin. Additionally, we thank Dr. Michael Bozack, Dr. Ram Gupta, and Dr. Anne Gorden for useful discussions. This work was supported by an U.S. Department of Education Graduate Assistance in Areas of National Need Fellowship, Grant #P200A060184.

Note Added after ASAP Publication. This article was published ASAP on July 22, 2009. A correction has been made in the Abstract. The correct version was published on July 29, 2009.

Supporting Information Available: SWNT TGA oxidation profiles, viscous oscillatory rheological responses, shear aggregation image, and oligomer structure. This material is available free of charge via the Internet at http://pubs.acs.org.

References and Notes

(1) Baughman, R. H.; Zakhidov, A. A.; de Heer, W. A. *Science* **2002**, *297* (5582), 787–792.
(2) Moniruzzaman, M.; Winey, K. I. *Macromolecules* **2006**, *39* (16), 5194–5205.
(3) Kota, A. K.; Cipriano, B. H.; Duesterberg, M. K.; Gershon, A. L.; Powell, D.; Raghavan, S. R.; Bruck, H. A. *Macromolecules* **2007**, *40* (20), 7400–7406.
(4) Vaia, R. A.; Wagner, H. D. *Mater. Today* **2004**, *7* (11), 32–37.
(5) Gojny, F. H.; Wichmann, M. H. G.; Köpke, U.; Fiedler, B.; Schulte, K. *Compos. Sci. Technol.* **2004**, *64* (15), 2363–2371.
(6) Miyagawa, H.; Drzal, L. T. *Polymer* **2004**, *45* (15), 5163–5170.
(7) Miyagawa, H.; Misra, M.; Mohanty, A. K. *J. Nanosci. Nanotechnol.* **2005**, *5* (10), 1593–1615.
(8) Lau, K.-T.; Hui, D. *Carbon* **2002**, *40* (9), 1605–1606.
(9) Schadler, L. S.; Giannaris, S. C.; Ajayan, P. M. *Appl. Phys. Lett.* **1998**, *73* (26), 3842–3844.
(10) Krishnamoorti, R.; Vaia, R. A. *J. Polym. Sci., Part B: Polym. Phys.* **2007**, *45* (24), 3252–3256.
(11) Fan, Z. H.; Advani, S. G. *J. Rheol.* **2007**, *51* (4), 585–604.
(12) Thess, A.; Lee, R.; Nikolaev, P.; Dai, H. J.; Petit, P.; Robert, J.; Xu, C. H.; Lee, Y. H.; Kim, S. G.; Rinzler, A. G.; Colbert, D. T.; Scuseria, G. E.; Tomanek, D.; Fischer, J. E.; Smalley, R. E. *Science* **1996**, *273* (5274), 483–487.
(13) O'Connell, M. J.; Bachilo, S. M.; Huffman, C. B.; Moore, V. C.; Strano, M. S.; Haroz, E. H.; Rialon, K. L.; Boul, P. J.; Noon, W. H.; Kittrell, C.; Ma, J.; Hauge, R. H.; Weisman, R. B.; Smalley, R. E. *Science* **2002**, *297* (5581), 593–596.
(14) Girifalco, L. A.; Hodak, M.; Lee, R. S. *Phys. Rev. B* **2000**, *62* (19), 13104–13110.
(15) Sun, C. H.; Yin, L. C.; Li, F.; Lu, G. Q.; Cheng, H. M. *Chem. Phys. Lett.* **2005**, *403* (4−6), 343–346.
(16) Sabba, Y.; Thomas, E. L. *Macromolecules* **2004**, *37* (13), 4815–4820.
(17) Bergin, S. D.; Nicolosi, V.; Streich, P. V.; Giordani, S.; Sun, Z. Y.; Windle, A. H.; Ryan, P.; Niraj, N. P. P.; Wang, Z. T. T.; Carpenter, L.; Blau, W. J.; Boland, J. J.; Hamilton, J. P.; Coleman, J. N. *Adv. Mater.* **2008**, *20* (10), 1876–1881.
(18) Tasis, D.; Tagmatarchis, N.; Bianco, A.; Prato, M. *Chem. Rev.* **2006**, *106* (3), 1105–1136.
(19) Dyke, C. A.; Tour, J. M. *J. Phys. Chem. A* **2004**, *108* (51), 11151–11159.
(20) Banerjee, S.; Hemraj-Benny, T.; Wong, S. S. *Adv. Mater.* **2005**, *17* (1), 17–29.
(21) Du, F.; Scogna, R. C.; Zhou, W.; Brand, S.; Fischer, J. E.; Winey, K. I. *Macromolecules* **2004**, *37* (24), 9048–9055.
(22) Rai, P. K.; Parra-Vasquez, A. N. G.; Chattopadhyay, J.; Pinnick, R. A.; Liang, F.; Sadana, A. K.; Hauge, R. H.; Billups, W. E.; Pasquali, M. *J. Nanosci. Nanotechnol.* **2007**, *7* (10), 3378–3385.
(23) Davis, V. A.; Ericson, L. M.; Parra-Vasquez, A. N. G.; Fan, H.; Wang, Y. H.; Prieto, V.; Longoria, J. A.; Ramesh, S.; Saini, R. K.; Kittrell, C.; Billups, W. E.; Adams, W. W.; Hauge, R. H.; Smalley, R. E.; Pasquali, M. *Macromolecules* **2004**, *37* (1), 154–160.
(24) Hough, L. A.; Islam, M. F.; Janmey, P. A.; Yodh, A. G. *Phys. Rev. Lett.* **2004**, *93* (16).
(25) Marceau, S.; Dubois, P.; Fulchiron, R.; Cassagnau, P. *Macromolecules* **2009**, *42* (5), 1433–1438.
(26) Duggal, R.; Pasquali, M. *Phys. Rev. Lett.* **2006**, *96* (24), 246104–4.
(27) Yakobson, B. I.; Couchman, L. S. Carbon Nanotubes: Supramolecular Mechanics. In *Dekker Encyclopedia of Nanoscience and Nanotechnology*; Schwarz, J. A., Contescu, C. I., Putyera, K., Eds.; Marcel Dekker: New York, 2004; pp 587−601.
(28) Hobbie, E. K.; Fry, D. J. *J. Chem. Phys.* **2007**, *126* (12).
(29) Kinloch, I. A.; Roberts, S. A.; Windle, A. H. *Polymer* **2002**, *43* (26), 7483–7491.
(30) Huang, Y. Y.; Ahir, S. V.; Terentjev, E. M. *Phys. Rev. B* **2006**, *73* (12).
(31) Sandler, J. K. W.; Kirk, J. E.; Kinloch, I. A.; Shaffer, M. S. P.; Windle, A. H. *Polymer* **2003**, *44* (19), 5893–5899.
(32) Rahatekar, S. S.; Koziol, K. K. K.; Butler, S. A.; Elliott, J. A.; Shaffer, M. S. P.; Mackley, M. R.; Windle, A. H. *J. Rheol.* **2006**, *50* (5), 599–610.
(33) Gojny, F. H.; Wichmann, M. H. G.; Fiedler, B.; Schulte, K. *Compos. Sci. Technol.* **2005**, *65* (15−16), 2300–2313.
(34) Wichmann, M.; Sumfleth, J.; Fiedler, B.; Gojny, F.; Schulte, K. *Mech. Compos. Mater.* **2006**, *42*, 395–406.
(35) Ma, W. K. A.; Chinesta, F.; Ammar, A.; Mackley, M. R. *J. Rheol.* **2008**, *52* (6), 1311–1330.
(36) Rodriguez, F. In *Principles of Polymer Systems*; Rodriguez, F., Ed.; Taylor & Francis: New York, 2003; p 4.
(37) Battisti, A.; Skordos, A. A.; Partridge, I. K. *Compos. Sci. Technol.* **2009**, *69* (10), 1516–1520.
(38) Seyhan, A. T.; Gojny, F. H.; Tanoglu, M.; Schulte, K. *Eur. Polym. J.* **2007**, *43* (7), 2836–2847.
(39) Seyhan, A. T.; Gojny, F. H.; Tanoglu, M.; Schulte, K. *Eur. Polym. J.* **2007**, *43* (2), 374–379.
(40) Thostenson, E. T.; Ziaee, S.; Chou, T.-W. *Compos. Sci. Technol.* **2009**, *69* (6), 801–804.
(41) Xu, Y. Q.; Peng, H.; Hauge, R. H.; Smalley, R. E. *Nano Lett.* **2005**, *5* (1), 163–168.
(42) Bozack, M. J. *Surf. Sci. Spectra* **1994**, *3* (1), 82–85.
(43) Bozack, M. J.; Zhou, Y.; Worley, S. D. *J. Chem. Phys.* **1994**, *100* (11), 8392–8398.
(44) Moreno-Castilla, C.; Lopez-Ramon, M. V.; Carrasco-Marin, F. *Carbon* **2000**, *38* (14), 1995–2001.
(45) Jimenez, G. A.; Jana, S. C. *Carbon* **2007**, *45* (10), 2079–2091.
(46) Hou, P. X.; Bai, S.; Yang, Q. H.; Liu, C.; Cheng, H. M. *Carbon* **2002**, *40* (1), 81–85.
(47) Zielke, U.; Huttinger, K. J.; Hoffman, W. P. *Carbon* **1996**, *34* (8), 983–998.
(48) Yue, Z. R.; Jiang, W.; Wang, L.; Gardner, S. D.; Pittman, C. U. *Carbon* **1999**, *37* (11), 1785–1796.
(49) Sato, J.; Breedveld, V. *Appl. Rheol.* **2005**, *15* (6), 390–397.
(50) Trappe, V.; Weitz, D. A. *Phys. Rev. Lett.* **2000**, *85* (2), 449–452.

(51) Dondero, W. E.; Gorga, R. E. *J. Polym. Sci., Part B: Polym. Phys.* **2006**, *44* (5), 864–878.
(52) Martin, C. A.; Sandler, J. K. W.; Shaffer, M. S. P.; Schwarz, M. K.; Bauhofer, W.; Schulte, K.; Windle, A. H. *Compos. Sci. Technol.* **2004**, *64* (15), 2309–2316.
(53) Sahimi, M.; Arbabi, S. *Phys. Rev. B* **1993**, *47* (2), 703.
(54) Hu, G.; Zhao, C.; Zhang, S.; Yang, M.; Wang, Z. *Polymer* **2006**, *47* (1), 480–488.
(55) Davis, V. A. Phase Behavior and Rheology of Single-Walled Carbon Nanotubes (SWNTs) in Superacids with Application to Fiber Spinning. Ph.D. Thesis, Rice University, **2006**.
(56) Kota, A. K.; Cipriano, B. H.; Powell, D.; Raghavan, S. R.; Bruck, H. A. *Nanotechnology* **2007**, *18* (50), 505705.
(57) Mitchell, C. A.; Krishnamoorti, R. *Macromolecules* **2007**, *40* (5), 1538–1545.
(58) Garboczi, E. J.; Snyder, K. A.; Douglas, J. F.; Thorpe, M. F. *Phys. Rev. E* **1995**, *52* (1), 819.
(59) Doi, M.; Edwards, S. F. *The Theory of Polymer Dynamics*; Clarendon Press: Oxford, 1986.
(60) Chaouche, M.; Koch, D. L. *J. Rheol.* **2001**, *45* (2), 369–382.
(61) Israelachvili, J. N. *Intermolecular and Surface Forces*; Academic Press: London, 1991; p 177.
(62) Zakri, C.; Poulin, P. *J. Mater. Chem.* **2006**, *16* (42), 4095–4098.
(63) Lin-Gibson, S.; Pathak, J. A.; Grulke, E. A.; Wang, H.; Hobbie, E. K. *Phys. Rev. Lett.* **2004**, *92* (4), 048302.
(64) Larson, R. G. *The Structure and Rheology of Complex Fluids*; Oxford University Press: New York, 1999.
(65) Schmid, C. F.; Switzer, L. H.; Klingenberg, D. J. *J. Rheol.* **2000**, *44* (4), 781–809.
(66) Dresselhaus, M. S.; Dresselhaus, G.; Jorio, A.; Souza Filho, A. G.; Saito, R. *Carbon* **2002**, *40* (12), 2043–2061.
(67) Dresselhaus, M. S.; Dresselhaus, G.; Jorio, A. *J. Phys. Chem. C* **2007**, *111* (48), 17887–17893.
(68) Li, J.; Zhang, Y. *Physica E* **2005**, *28* (3), 309–312.
(69) Rinzler, A. G.; Liu, J.; Dai, H.; Nikolaev, P.; Huffman, C. B.; Rodríguez-Macías, F. J.; Boul, P. J.; Lu, A. H.; Heymann, D.; Colbert, D. T.; Lee, R. S.; Fischer, J. E.; Rao, A. M.; Eklund, P. C.; Smalley, R. E. *Appl. Phys. A: Mater. Sci. Process.* **1998**, *67* (1), 29–37.